ELSEVIER

Journal of Electroanalytical Chemistry 522 (2002) 2–10

Journal of Electroanalytical Chemistry

www.elsevier.com/locate/jelechem

Electrochemical and topological characterization of gold(111) | oligo(cyclohexylidene) | gold nanocrystal interfaces

F. Reincke [a], S.G. Hickey [a], J.J. Kelly [a], T.W. Braam [b], L.W. Jenneskens [b], D. Vanmaekelbergh [a,*]

[a] *Chemistry and Physics of Condensed Matter, Debye Institute, University of Utrecht, Princetonplein 1, 3584 CC Utrecht, The Netherlands*
[b] *Department of Physical Organic Chemistry, Debye Institute, University of Utrecht, Padualaan 8, 3584 CH Utrecht, The Netherlands*

Received 1 June 2001; received in revised form 1 October 2001; accepted 6 October 2001

Abstract

Self-assembled monolayers (SAMs) of functionalized oligo(cyclohexylidene) molecules on gold(111) surfaces have been studied by measurement of the interfacial capacitance in concentrated electrolyte solutions and by cyclic voltammetry with $Fe(CN)_6^{3-/4-}$ as the redox system. The morphology of the layers has been studied by scanning tunneling microscope (STM) and AFM. We found that sulfide-terminated oligo(cyclohexylidenes) form a well-ordered SAM on gold(111) and that the oxime end-functionality inhibits the formation of ordered SAMs. Charge-stabilized gold nanocrystals attach to sulfide-terminated SAMs on gold(111) to form robust gold(111) | oligo(cyclohexylidene) | gold nanocrystal molecular junctions. We show that the nanocrystal | water interface can be charged by electron transport through the molecular layer. © 2001 Published by Elsevier Science B.V.

Keywords: Gold(111); Jellium; Oligo(cyclohexylidene); Gold nanocrystals; Self-assembly; Nanostructured interface

1. Introduction

Electrical devices in which molecules or molecular crystals are the active element receive considerable interest from chemists and physicists since they are promising candidates for future miniaturized electrical components [1]. Single-molecule electrical junctions can be fabricated by mounting a molecule between two closely spaced electrodes immobilized on a non-conducting substrate. The fabrication of such a device is, however, still very demanding. Only a few single-molecule electrical devices have been presented [2–6]. An alternative method, which can be used for investigating electron transport through single molecules, is based on the attachment of the molecules by one end to a conducting substrate, while an electrical contact at the other end of the molecule is obtained with the tip of a scanning tunneling microscope (STM) [7]. Attaching a nanometer-sized particle with an optical or electrical function to the end of the molecule would be a further step in the fabrication of real molecular junctions. Recently, we have demonstrated that insulating CdS and CdSe quantum dots can be bound to the thiol or sulfide end-functionality of alkane and oligo(cyclohexylidene) molecules, which have been self-assembled on gold. This results in a parallel array of optically and electrically addressable gold | molecule | Q-dot junctions [8,9]. Schiffrin and colleagues reported a self-assembled array of individual and independent molecular junctions, terminated with a gold nanocrystal contact, which show on–off conductance, depending on the electron occupation of a built-in redox system acting as a switch [10].

Here, we report on an electrochemical and scanning probe microscopy (SPM) characterization of a nanostructured interface consisting of a parallel array of gold(111) | oligo(cyclohexylidene) | gold nanocrystal molecular junctions. End-functionalized oligo(cyclohexylidene) molecules (see Fig. 1 for structure and notation) form an interesting class of molecules for single-molecule electrical devices since: (i) molecules of different lengths and with a variety of end-functionali-

* Corresponding author. Tel.: +31-30-2532218; fax: +31-30-2532403.
E-mail address: daniel@phys.uu.nl (D. Vanmaekelbergh).

0022-0728/02/$ - see front matter © 2002 Published by Elsevier Science B.V.
PII: S0022-0728(01)00712-4

ties can be prepared; (ii) it will be shown that a number of these molecules form a well-ordered self-assembled monolayer (SAM) on gold(111); (iii) MO-theory and two different types of experiments have shown that they exhibit strong σ-through-bond coupling making them possible candidates for molecular wires [8].

We performed a layer-by-layer characterization. First, we investigated the possible formation of self-assembled mono- and difunctionalized oligo(cyclohexylidene) layers on Au(111) surfaces using classical electrochemical methods i.e. by measurement of the interfacial capacitance and by cyclic voltammetry in the presence of a redox system ($Fe(CN)_6^{3-/4-}$). We employed STM, contact- and tapping mode AFM to investigate the topology of the SAMs on gold. Second, the attachment of gold nanocrystals (Au_{NC}) to the molecular layers was studied by in-situ measurement of the electrochemical capacitance and by ex-situ AFM. We find that robust Au(111) | oligo(cyclohexylidene) | Au_{NC} molecular junctions can be prepared using oligo(cyclohexylidene) disulfides (Fig. 1b).

2. Experimental

Chemicals were obtained from Aldrich (pentamethylene sulfide 99%, hydrogen tetrachloroaurate(III) trihydrate, sodium citrate dihydrate 99%), Lancaster (1,4-dithiane 98%) and Merck (potassium chloride p.a., sodium perchlorate monohydrate p.a., potassium hexacyanoferrate(II) trihydrate p.a.). All solutions were made using purified water (16 MΩ cm) from the Purite Bio Select. The end-functionalized oligo(cyclohexylidenes) were prepared following previously published studies [11–14].

Au(111) electrodes were prepared by annealing a 200 nm thick gold layer evaporated on borosilicate glass in a hydrogen flame. STM images showed grains with a size in the 1 μm range, which expose atomically flat Au(111) surfaces with monoatomic steps. In order to prevent surface contamination, flame-annealed gold samples were immediately used as the working electrode in an electrochemical cell for further characterization, or immersed in an ethanolic solution of the specific oligo(cyclohexylidene) solution (50 °C for at least 2 days) for self-assembly.

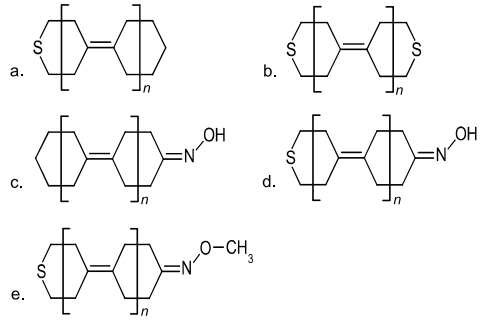

Fig. 1. The end-functionalized oligo(cyclohexylidene) molecules used in this study. For simplicity we refer to these molecules by their functional groups, viz. (a) monosulfide, (b) disulfide, (c) oxime, (d) oxime-sulfide, and (e) methylated oxime-sulfide. The oligo(cyclohexylidene) group (between square brackets) is repeated n times, where n is 0, 1 or 2. Structural analysis on single crystals and ab-initio calculations showed that these molecules preferentially stack in chair conformation [11–13]. Presumably, the molecules are stacked in a molecular layer in the same conformation.

The electrodes were placed in an electrochemical cell, together with a Pt counter and a calomel (SCE) reference electrode. All potentials mentioned in the text are with respect to the SCE. The electrolyte solution was kept at 25 °C and deaerated by argon. The EG&G 273A potentiostat/galvanostat and Solartron 1255B frequency response analyzer were operated by a home-made Labview program. The impedance data were fitted to a circuit consisting of a resistor R_Ω in series with a parallel circuit containing a capacitance C and a second resistor R_F. C was interpreted as the interfacial capacitance. All cyclic voltammograms were recorded at 100 mV s^{-1}. A Digital Instruments Nanoscope IIIa Multimode, run in STM and 'tapping mode'-AFM, was used to examine the topology of the electrodes.

Aqueous colloidal suspensions of charge-stabilized gold nanoparticles (diameter 16–20 nm) were made by citrate reduction of $HAuCl_4$ according to the method of Frens [15]. Diameters down to 5 nm were obtained by co-injecting varied amounts of 0.1% $NaBH_4$ along with the citrate. Colloid attachment was achieved by hanging the electrodes vertically in a freshly prepared nanoparticle solution. The electrodes were removed from solution with the gold facing down (to prevent Langmuir–Blodgett deposition of the nanoparticles) rinsed with water and dried before imaging with the AFM.

3. Results

3.1. Functionalized oligo(cyclohexylidenes) on Au(111)

We first investigated the possibility of forming SAMs with monofunctionalized oligo(cyclohexylidenes). Fig. 2a shows the interfacial capacitance of a bare gold(111) electrode in an aqueous 1 M KCl solution as a function of the electrode potential, together with the capacitance measured after application of the monosulfide (Fig. 1a with $n = 1$) and the oxime (Fig. 1c with $n = 1$). The frequency dependence of the measured capacitances at 0 V versus SCE is shown in the insert. The capacitance (normalized with respect to the capacitance at 1000 Hz) of the bare electrode increases considerably with decreasing modulation frequency. A strong frequency dependence of the interfacial capacitance in concentrated aqueous electrolytes has been reported before [16]. This

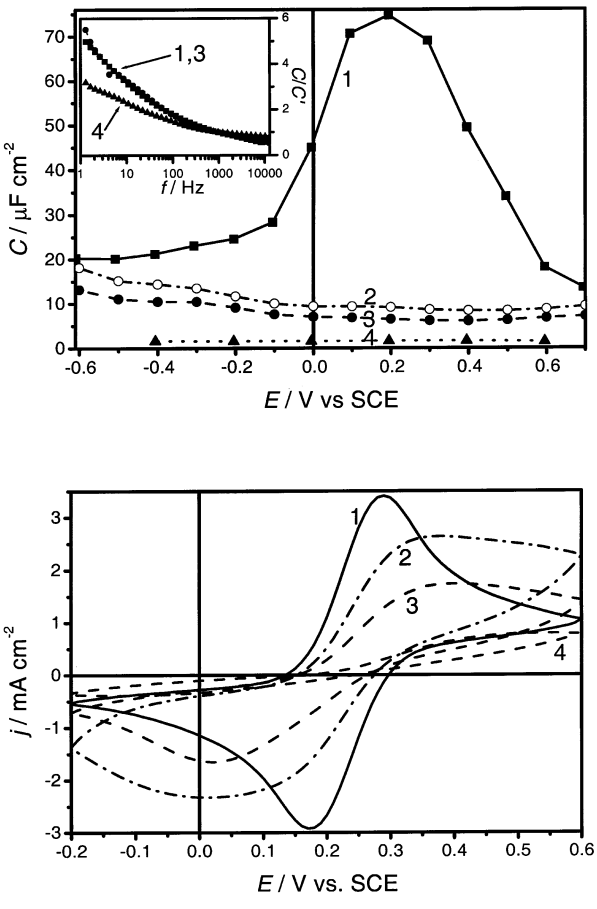

Fig. 2. (a) The interfacial capacitance (measured at 1000 Hz) of a gold(111) electrode in an aqueous solution of 1 M KCl at 25 °C as a function of electrode potential after pretreatment with ethanolic solutions of oligo(cyclohexylidenes) with different end-functionalities. (1, —■—) an unpretreated, bare gold(111) electrode; (2, –○–) after immersion in a pure ethanol solution for 12 h; (3,– – ● – –) after immersion in an oxime | ethanol (Fig. 1c; $n = 1$) solution for 24 h; (4, ···▲···) after immersion in a monosulfide | ethanol (Fig. 1a; $n = 1$) solution for 24 h. The inset shows the capacitance C at 0 V versus SCE (normalized with respect to that measured at 1000 Hz, denoted C') as a function of the modulation frequency. (b) Cyclic voltammograms measured in a 10 mM $Fe(CN)_6^{4-}$/1 M KCl solution after several pretreatments. (1, —) an unpretreated, bare gold(111) electrode; (2,– –) after immersion in a pure ethanol solution for 12 h; (3, - - -) after immersion in an oxime | ethanol (Fig. 1c; $n = 1$) solution for 24 h; (4, ·····) after immersion in a monosulfide | ethanol (Fig. 1a; $n = 1$) solution for 24 h.

frequency dispersion is most likely due to surface roughness [17] and/or specific adsorption of the anion [18,19]. It was not possible to account for the frequency dependence by a constant phase element. We, therefore, present the capacitance measured at a frequency of 1000 Hz for further discussion. The bare Au(111) electrode shows a pronounced maximum at $+0.2$ V, close to the potential of zero charge. The maximum capacitance in a 1 M KCl solution varied from sample to sample (68 μF $cm^{-2} \pm 15\%$ at 1000 Hz). Negative with respect to the maximum, the capacitance decreased to a constant value equal to 20 μF cm^{-2}. Positive of the potential of zero charge the capacitance decreased and reached a constant value of 9–15 μF cm^{-2} at 0.7 V. The capacitance plot of Au(111) in 1 M $KClO_4$ has the same features, the maximum in the capacitance is observed at $+0.3$ V versus SCE, which is close to the point of zero charge E_{pzc} of $+0.33$ V versus SCE found in the literature [20–24]. The C versus E plot shows an asymmetric peak in KCl, very probably due to chemisorption of Cl^- ions at the electrode surface in the potential range positive of E_{pzc}. Similar results (an increase of the maximum capacitance and shift of the maximum to more negative potentials with increasing specific adsorption) have been reported in the literature [16,18,19].

The capacitance of the gold electrode measured in a 1 M KCl solution after a prolonged immersion in an ethanolic solution of oxime (Fig. 1c; $n = 1$) is considerably reduced compared with that of a bare electrode, and a peak is not found in the capacitance–potential curve. A similar reduction of the interfacial capacitance is, however, found after placing the electrode overnight in a pure ethanol solution. Note that the frequency dependence of the interfacial capacitance of a bare and an oxime-treated electrode is identical (insert Fig. 2a). We infer that the interfacial capacitance is reduced with respect to that of a bare electrode due to physisorption of ethanol or oxime molecules and that a robust SAM is not formed. In contrast, the capacitance of the gold electrode in a 1 M KCl solution is extremely low ($C < 1$ μF cm^{-2}) in the entire potential range after application of a monosulfide (Fig. 1a; $n = 1$). The capacitance decreases with increasing length of the monosulfide (Fig. 1a; $n = 0$, 1). This is at odds with what was found with functionalized n-alkanethiol SAMs [25–27]. This indicates that monosulfides form well-ordered SAMs that cover the entire electrode. This has been confirmed by ex-situ tapping mode AFM and STM characterization of such layers. No defects in the layers could be found, and the atomic steps of the Au(111) surface were visible on the images.

The contrast between the effect of oximes and monosulfides (Fig. 1c and a, respectively) on Au(111) is also illustrated by the cyclic voltammograms shown in Fig. 2b. With the bare gold electrode the potential difference between the reduction and oxidation peaks of $Fe(CN)_6^{3-/4-}$ in a 1 M KCl solution is 110 mV, whereas 58 mV is expected for a reversible reaction. The reaction is thus quasi-reversible at a scan rate of 100 mV s^{-1}. Similar results have been reported in the literature [28]. After immersion of the gold sample in ethanol or an oxime in ethanol solution, the reaction becomes more irreversible, indicating that oxime or ethanol molecules (partly) cover the electrode surface. However, the cyclic voltammogram tends to that of a bare electrode when the electrode potential is scanned

for a longer time, indicating that the ethanol or oxime molecules are weakly physisorbed and can be removed electrochemically. On the other hand, when the gold electrode was treated with a monosulfide (Fig. 1a; $n = 1$) dissolved in ethanol, the oxidation/reduction reaction is strongly inhibited with respect to that at a bare gold electrode. Pinholes in the SAM are rarely observed with STM; thus it is likely that the remaining Faradaic current is due to electron transfer through the oligo(cyclohexylidene) SAM. We conclude that monosulfide oligo(cyclohexylidenes) form well-ordered SAMs, with a strong gold–S bond. It is clear that the oxime function does not bind chemically to gold.

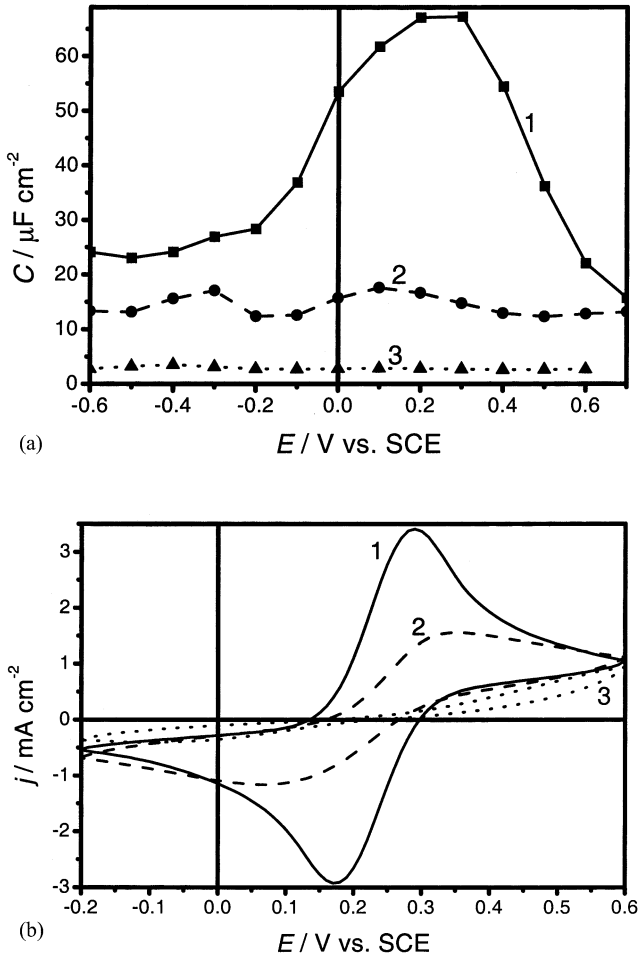

Fig. 3. (a) The interfacial capacitance (measured at 1000 Hz) of a gold(111) electrode in an aqueous solution of 1 M KCl at 25 °C as a function of electrode potential after pretreatment with ethanolic solutions of oligo(cyclohexylidenes) with different end-functionalities. (1, —■—) an unpretreated, bare gold(111) electrode; (2, – – ● – –) after immersion in a oxime-sulfide | ethanol (Fig. 1d; $n = 0$) solution for over 48 h; (3, ··▲··) after immersion in a methylated oxime-sulfide | ethanol (Fig. 1e; $n = 0$) solution for 24 h. (b) Cyclic voltammograms measured in a 10 mM $Fe(CN)_6^{4-}$/1 M KCl solution after different pretreatments. (1,—) an unpretreated, bare gold(111) electrode; (2,– – –) after immersion in a oxime-sulfide | ethanol (Fig. 1d; $n = 0$) solution for over 48 h; (3, ·····) after immersion in a methylated oxime-sulfide | ethanol (Fig. 1e; $n = 0$) solution for 24 h.

Next, we investigated the possible formation of SAMs by difunctionalized oligo(cyclohexylidenes), i.e. disulfides, oxime-sulfides and methylated oxime-sulfides, on Au(111). After treatment of the gold surface with a disulfide (Fig. 1b; $n = 0$), the interfacial capacitance in 1 M KCl reduces to a value of about 6 μF cm^{-2} at 1000 Hz, independent of the electrode potential. In addition, the cyclic voltammograms show a strong attenuation of interfacial electron transfer. This points to the formation of a well-ordered oligo(cyclohexylidene) disulfide SAM covering the entire gold surface; this conclusion is supported by AFM measurements. The results obtained after application of the oxime-sulfides (Fig. 1d; $n = 0$) and methylated oxime-sulfides (Fig. 1e; $n = 0$) are shown in Fig. 3a and b. After application of the oxime-sulfide, the capacitance is moderately reduced with respect to that of a bare gold electrode measured in KCl solution. The capacitance is in the range of 15–20 μF cm^{-2} where a value smaller than 10 μF cm^{-2} is expected for a well-ordered SAM. Moreover, the $Fe(CN)_6^{3-/4-}$ peak currents in the voltammogram for a 1 M KCl solution are reduced to only half the values found with a bare electrode. These results suggest that oxime-sulfides do not form a well-ordered SAM on Au(111). This is unexpected, since the sulfide function binds strongly to gold, resulting in well-ordered SAMs with the mono- and disulfide. The oxime =N–OH function seems to hinder SAM formation. This is supported by the results shown in Fig. 3a and b, obtained with methylated oxime-sulfides (Fig. 1e; $n = 0$). The capacitance reduces to a value of 4 μF cm^{-2} at 1000 Hz, even slightly lower than that of a disulfide. In addition, the reduction/oxidation of the $Fe(CN)_6^{3-/4-}$ redox system is strongly inhibited. It is not yet clear why the =N–OH end-functionality has such a strong poisoning effect in the formation of a SAM layer. It may be related to the fact that the =N–OH group can form hydrogen bonds with ethanol or another oxime molecule.

3.2. Formation and characterization of *Au(111) | oligo(cyclohexylidene) | Au_{NC} interfaces*

We investigated whether the gold(111) | disulfide system can be used in preparing gold(111) | oligo-(cyclohexylidene) | Au_{NC} molecular junctions. Charge-stabilized gold nanocrystals (5–20 nm in size) were adsorbed on a gold(111) | disulfide interface from an aqueous colloidal suspension [15]. The size of the nanocrystals was checked by UV–vis spectroscopy, TEM and tapping mode AFM. Fig. 4a shows a tapping-mode AFM picture of a Au | disulfide interface which is covered with Au_{NC}, from the cross-section (inset) it follows that the height of the Au-nanoparticles is 15 nm which is in agreement with the particle size in solution. The same agreement was found for a

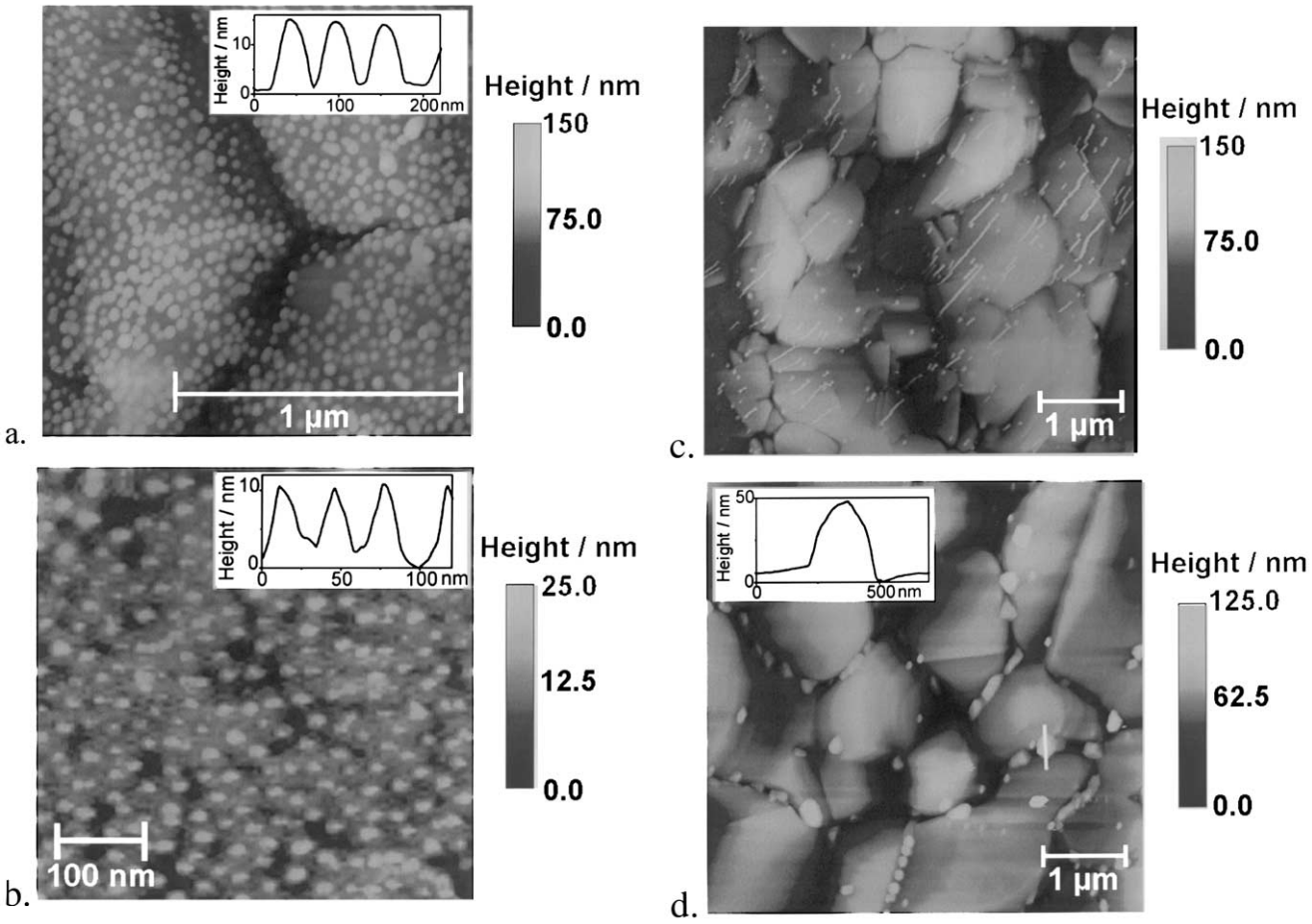

Fig. 4. Tapping mode AFM images in ambient air of oligo(cyclohexylidene)-covered and bare Au(111) surfaces after immersion in an aqueous colloidal solution of charge-stabilized gold nanoparticles (size 5–20 nm). Left: height image. Right: amplitude image. (a) A gold(111) surface covered with a disulfide ($n = 0$) SAM after immersion for 4 h in the colloidal gold solution (diameter 16 nm). Individual gold nanocrystals are attached to the SAM. The size of the particles is deconvoluted by the tip in the in-plane (X–Y) directions. The height of the particle forms a good estimate of the particle size (see inset). (b) Same as (a), but with 8 nm gold particles. (c) A gold(111) surface covered with a monosulfide ($n = 0$) SAM after immersion for 1 h in 16 nm colloidal gold solution. The stripes are due to the displacement of gold nanocrystals by the AFM tip (from top-right to bottom-left) until they are immobilized at a grain boundary. A bare gold(111) surface after immersion in a 16 nm colloidal gold solution for 1 h. Au nanocrystals do not attach to the (III) surface. Some agglomerates ($\gg 20$ nm) can be seen at the grain boundaries.

Au | disulfide | Au_{NC} interface with Au nanocrystals of 8 nm in size, see Fig. 4b. Interestingly, the nanocrystals attach as individual particles to the disulfide SAM; no clustering is observed. The nanocrystals cannot be moved along the surface by the tapping-mode tip indicating strong bonding and formation of a robust Au(111) | disulfide | Au_{NC} junction. Charge-stabilized nanocrystals were also observed to adhere to some extent to an alkyl-terminated monosulfide (Fig. 1a; $n = 0$) SAM. Fig. 4c shows the result after immersion of the gold with a monosulfide SAM in colloidal suspension. Individual nanocrystals are observed on the SAM. However, when the tip/substrate interaction is increased (low setpoint) the gold nanocrystals can be moved along the surface by the tapping-mode tip, indicating that they are van der Waals-bound to the surface. Interestingly, charge-stabilized gold nanocrystals do not attach at a bare Au(111) surface under open-circuit conditions. The result of prolonged immersion of bare gold in a colloidal solution is shown in Fig. 4d: only some large agglomerates are visible at the grain boundaries.

We characterized the Au(111) | disulfide | Au_{NC} interface in a 1 M KCl solution by charging/discharging the interface with a small-amplitude potential step (between E and $E + \Delta E$). We present the results as the low-frequency limit of the interfacial capacitance $C(\omega \to 0, E) = \Delta\sigma(E)/\Delta E$, ($\Delta\sigma(E)$ being the measured charge per unit surface area) after confirming that the results are independent of the amplitude of the potential step for $\Delta E \leq 0.05$ V. Fig. 5 shows that the interfacial capacitance is considerably reduced compared with that of a bare electrode after application of the disulfide to the Au(111) surface, again demonstrating the quality of the disulfide SAM on gold. When gold nanocrystals are anchored to the SAM, the capacitance increases in

the entire potential range; the increase is most pronounced around the potential of zero charge; the capacitance of the nanostructured Au (111) | disulfide | Au_{NC} interface shows a maximum as a function of the potential, similar to that of a bare gold electrode. We conclude that the attachment of gold nanocrystals to the SAM leads to the formation of an additional gold | water interface which can be charged/discharged by electron transfer through the molecular layer. A simple model to explain this effect qualitatively will be discussed below.

We used the increase of the interfacial capacitance $C(\omega \to 0,\ E \approx E_{pzc}$ as a quantitative measure to follow in real time and in-situ (i.e. in the colloidal gold suspension) the anchoring of gold nanocrystals (15 nm in size) to a gold | disulfide SAM (see Fig. 6). A justification of this procedure is given in the discussion. Initially, the surface concentration of Au_{NC} on the SAM layer increases linearly with time; the addition rate decreases at longer times and finally becomes almost zero. We note that the maximum coverage observed in the saturation region is about 75 particles μm^{-2}, corresponding to an average center to center distance of about 97 nm between two nanocrystals. A local mapping is given in the inset of Fig. 4a. In Fig. 6 the relative increase in capacitance $\Delta C/\Delta C_{max}$, which is a measure for the relative surface coverage θ, is plotted versus time. A fit of the addition kinetics corresponding to $d\theta/dt = k_a(1-\theta) - k_d\theta$ (θ being the fraction of the surface sites occupied by a nanocrystal, k_a and k_d are the pseudo-first order rate constants for nanoparticle adsorption and desorption, respectively) is included in the figure. It can be seen that this law describes well the kinetics of particle addition. It should be noted that the attachment of gold nanocrystals is likely to be an irreversible process, i.e. $k_d \cong 0$. This may also explain why the gold nanocrystals do not form ordered two-dimensional arrays on the gold | disulfide surface.

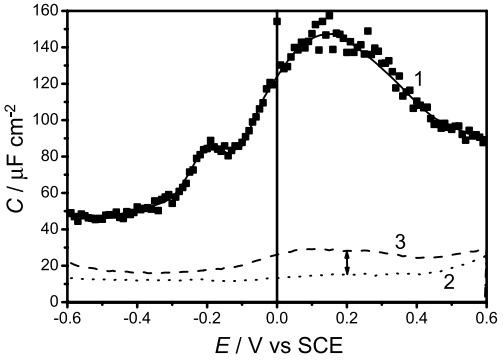

Fig. 5. The low-frequency limit of the interfacial capacitance of a gold(111) electrode after different pretreatments in a 1 M KCl solution at 25 °C as a function of the electrode potential. The capacitance was obtained from the charging/discharging response to a small-amplitude potential step. (1, —■—) an unpretreated, bare gold(111) electrode; (2, ···) after immersion of the gold(111) electrode in an ethanolic solution of disulfide (Fig. 1b; $n = 0$); (3,– – –) after immersion of the gold(111) | disulfide electrode in an aqueous colloidal gold nanocrystal suspension for 4 h. The ↕ shows the increase in the capacitance due to the gold nanoparticle attachment.

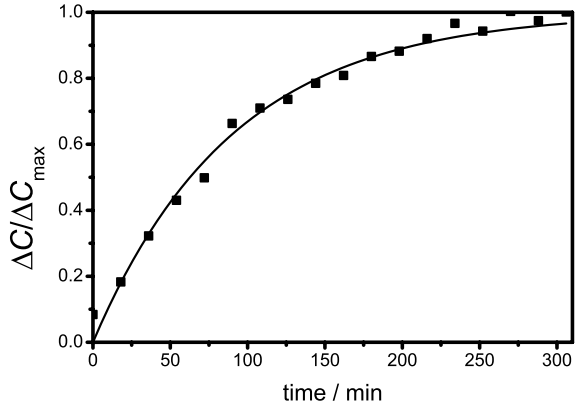

Fig. 6. The relative surface coverage θ of gold nanocrystals on a gold(111) | disulfide (Fig. 1b; $n = 0$) SAM attachment obtained from the increase in the interfacial capacitance (see arrow in Fig. 5) measured in-situ during nanocrystal attachment. The line shows a fit according to $d\theta/dt = k_a(1-\theta) - k_d\theta$.

4. Discussion and conclusions

The interfacial capacitance of a gold(111) electrode covered with an oligo(cyclohexylidene) SAM is very much reduced compared with that of a bare gold electrode; in addition it shows a different dependence on the electrode potential and modulation frequency. The capacitance features change again when gold nanocrystals become attached to the SAM. The highly polarizable double layer structure (i.e. jellium layer) of the metal, itself arising from electrons that spill over the surface layer of gold core ions, plays a key role in the total capacitance [29,30]. There is still debate on the applicability of the jellium model to noble metals. Here, we take the jellium model as a basis to rationalize the experimental results presented in the foregoing section.

The capacitance of a bare gold(111) electrode measured in 1 M KCl and 1 M $KClO_4$ aqueous solutions shows a pronounced and asymmetric peak as a function of the electrode potential and a relatively strong frequency dependence. The peak can be accounted for by the capacitance of the metal double layer C_M that is in series with the capacitance of the first water layer C_{sol}, see Fig. 7a. The capacitance of the metal double layer can be written as

$$C_M = \frac{\partial \sigma}{\partial(\varphi_M - \varphi_S)} \quad (1)$$

in which $\varphi_M - \varphi_S$ is the electrostatic potential difference between the bulk metal and a position just outside the electron spill-over region, and σ is the charge density on the metal. An incremental increase of the

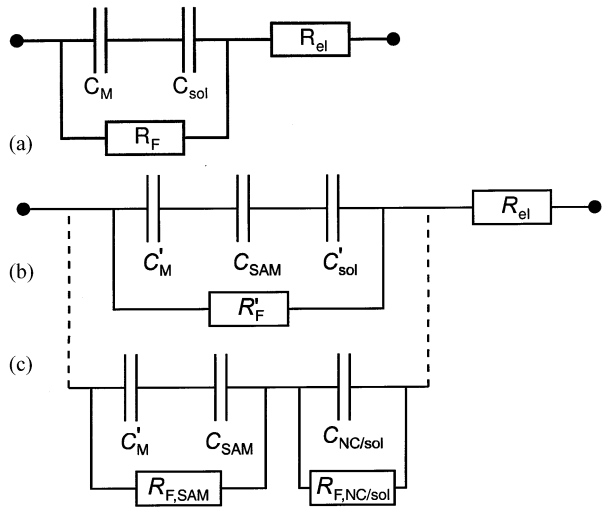

Fig. 7. Electrical equivalent circuits representing the interfacial structure of bare and nanostructured gold(111) electrodes for concentrated aqueous electrolytes. (a) Interface of a bare gold(111) electrode consisting of a jellium surface layer (capacitance C_M) and an ordered water layer (C_{sol}). (b) Interface of a oligo(cyclohexylidene) SAM covered gold(111) electrode. The molecular layer has a capacitance C_{SAM}. (c) Equivalent circuit for a site at which a gold nanocrystal is attached to the SAM. The nanocrystal | electrolyte interface can be charged/discharged through the oligo(cyclohexylidene) molecules ($R_{F,SAM}$). The complete equivalent circuit of a gold(111) | oligo (cyclohexylidene) | gold nanocrystal interface can be obtained by placing circuits b and c in parallel.

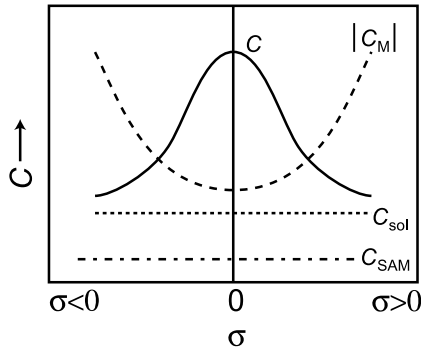

Fig. 8. A sketch of the dependence of the individual capacitances shown in Fig. 7 on the surface charge density σ. The interfacial capacitance $C = |C_M|C_{sol}/|C_M| - C_{sol}$ of a bare gold electrode (see Fig. 7a) shows a pronounced maximum close to $\sigma = 0$. The interfacial capacitance of a SAM covered gold electrode $C = |C_M|C_{SAM}/|C_M| - C_{SAM}$ tends to C_{SAM} (see text).

positive charge density reduces the width of the spill-over region and decreases $\varphi_M - \varphi_S$; thus, $C_M < 0$ [29,30]. The metal double layer shows a maximum polarizability around the point of zero charge density $\sigma = 0$. As a result $|C_M|$ has a minimum around E_{pzc} (Fig. 8). The interfacial capacitance of a bare gold electrode is then given by:

$$C = \frac{|C_M|C_{sol}}{|C_M| - C_{sol}} \quad (2)$$

The peak in the interfacial capacitance C around E_{pzc} is rationalized by assuming (i) that C_{sol} does not depend strongly on the charge density and hence on the electrode potential, and (ii) that $|C_M| - C_{sol}$ is positive in the entire potential region and has a minimum around E_{pzc}. The maximum interfacial capacitance depends sensitively on the difference $|C_M| - C_{sol}$ around the point of zero charge. This explains the strong influence of the nature of the metal and exposed crystal surface on the maximum interfacial capacitance close to E_{pzc}, reported in the literature [30]. In 1 M KCl and 1 M $KClO_4$, E_{pzc} is $+0.2$ and $+0.3$ V versus SCE, respectively. This is somewhat more negative than in fluoride electrolytes ($E_{pzc} = +0.33$ V vs. SCE [20–24]) indicating specific Cl^- and to lesser extent ClO_4^- adsorption on the gold(111) surface. The frequency dispersion of a bare electrode is more pronounced than that of a gold electrode covered with a SAM (see insert of Fig. 2a). This suggests that the frequency dispersion of bare gold electrodes is due partly to anion adsorption [19]. At potentials negative with respect to E_{pzc} the capacitance of the bare electrode reduces to a nearly constant value of 20 μF cm^{-2} at 1000 Hz, indicating that $C_M \gg C_{sol} \cong 20$ μF cm^{-2} when the charge density on the gold surface is negative (see also Fig. 8).

Oligo(cyclohexylidene) mono- and disulfide molecules, and methylated oxime-sulfide molecules (Fig. 1a, b and e, respectively) form well-ordered SAMs on gold(111) surfaces, characterized by a low and nearly potential-independent capacitance ($C \leq 6$ μF cm^{-2}). The structure of the double layer is schematically presented in Fig. 7b. The capacitance of the metal double layer can be influenced by the large density of Au–S bonds; C'_M is used instead of C_M to denote this capacitance. Similarly, we use C'_{sol} (instead of C_{sol}) for the capacitance of the solvent layer in contact with the SAM. The total interfacial capacitance is now given by:

$$C = \frac{|C'_M|C'_{sol}C_{SAM}}{|C'_M|(C'_{sol} + C_{SAM}) - C_{SAM}C'_{sol}} \quad (3)$$

The interfacial capacitance is nearly equal to that of the SAM monolayer for the case in which $C'_M > C_{sol} > C_{SAM}$:

$$C \cong C_{SAM} = \frac{\varepsilon_{SAM}\varepsilon_0}{d_{SAM}} \quad (4)$$

where ε_{SAM} is the dielectric constant and d_{SAM} the thickness of the SAM. Eq. (4) explains why the observed capacitance of the SAM covered gold electrode is low and does not show a peak around E_{pzc}. We should remark here that there are subtle, but reproducible differences between sulfide-oligo(cyclohexylidenes) of the same length ($n = 0$, 1) but with different end-functionalities at the water side; the capacitance of the alkyl-terminated SAM is smaller than that of a methylated oxime-sulfide (Fig. 1e) terminated SAM,

which is, in turn, slightly smaller than that of a sulfide-terminated (Fig. 1b) SAM. This may be due partly to a difference in ε_{SAM}, partly to a different ordering of the first water layers contacting the hydrophobic and less hydrophobic end-functionalities of these oligo(cyclohexylidene) molecules. A dependence on the end-functionality has also been reported in the literature [25,26]. We also note that the capacitance decreases with increasing length of the molecules in the SAM, which is in qualitative agreement with Eq. (4).

When a gold nanocrystal Au_{NC} is anchored to an S-terminated oligo(cyclohexylidene) SAM layer a nanometer-sized electrical junction is formed with an impedance represented in Fig. 7c. This impedance replaces that of a non-occupied site shown in Fig. 7b. Since the entire system consists of both occupied and non-occupied sites, the total electrical equivalent circuit for the Au(111) | oligo(cyclohexylidene) | Au_{NC} interface is formed by a parallel connection of Fig. 7b and c. The impedance of a gold(111) | oligo(cyclohexylidene) | Au_{NC} | water structure shown in Fig. 7c accounts for charging of the gold nanocrystal through the molecular SAM layer (Faradaic resistance $R_{F,SAM}$) and the formation of an electrochemical double layer at the gold nanocrystal | water interface (capacitance $C_{NC/sol}$). At sufficiently low frequencies, the nanocrystal | water interface can be charged/discharged, and the interfacial capacitance will be larger than that of a gold(111) | oligo(cyclohexylidene) | water site. Although the scheme presented in Fig. 7b and c for the nanostructured interface is perhaps naïve, it can be used to understand the increase of the interfacial capacitance of the gold electrode upon attachment of gold nanocrystals to the SAM layer (Figs. 5 and 6).

From the above discussion, we may conclude that the electrochemical capacitance provides a plausible description of a bare gold(111) | water, a gold(111) | oligo(cyclohexylidene) | water and a gold(111) | oligo(cyclohexylidene) | Au_{NC} | water interface. The self-assembly of end-functionalized alkane molecules on metals surfaces (mostly alkanethiols on gold surfaces) has been studied extensively by other research groups [7,31,32]; similar conclusions concerning the usefulness of electrochemistry have been drawn. The novelty of our work lies in the choice of the molecules, i.e. oligo(cyclohexylidenes), and in the striking effects found with different end-functionalities. Oligo(cyclohexylidene) molecules have a rigid C-skeleton with a chair conformation. This enables the formation of well-ordered SAMs, even with short molecules, with one cyclohexyl ring (i.e. $n = 0$). In addition, both chemical end-functionalities play a key role in the possible formation of oligo(cyclohexylidene) SAMs on gold(111) surfaces. We found that oligo(cyclohexylidene) molecules terminated with one or two sulfide-end functions form well-ordered SAMs on gold(111). Even the shortest oligo(cyclohexylidene) molecule led to a low and potential-independent capacitance and a considerable reduction of the rate of interfacial electron transfer. The electrochemical results show that oxime-terminated oligo(cyclohexylidene) molecules do not form a SAM on gold(111). The oxime–gold interaction is too weak. Surprisingly, oligo(cyclohexylidene) molecules with a sulfide and oxime function also do not form well-ordered SAMs. This is not well understood at present, but the results clearly indicate that the oxime termination inhibits the formation of well-ordered layers.

A second new aspect in this work is that we show that the attachment of Au nanocrystals to a gold-oligo(cyclohexylidene) SAM can be followed in-situ by measurement of the interfacial capacitance. Attachment of a gold nanocrystal to the SAM leads to a new gold | water nanointerface that can be charged by electron transport through the molecular layer. Similarly, photo-induced electron transfer through oligo(cyclohexylidene) molecules mounted between an insulating quantum dot and gold has been observed [8]. By measurement of this additional charge, we were able to follow the adsorption kinetics. A simple law is found; the rate of adsorption of the nanocrystals on the SAM is proportional to the density of free sites on the SAM surface. Under conditions of saturation, we find with tapping mode STM, a disordered array of individual gold nanocrystals, still corresponding to a relatively low coverage. Most likely, the attachment of nanocrystals is an irreversible process. The low coverage may be due to the charged double layer around the nanocrystals. This also explains why there is no clustering of individual nanocrystals. It should be noted here that charge-stabilized gold nanocrystals do not attach to bare gold, but only form some clusters at the grain boundaries. We suggest that the electron spill-over region (jellium layer) of the bare gold(111) surface repels the negatively charged gold nanocrystals. Interestingly, when the gold(111) surface is covered with an alkyl-terminated SAM, gold nanocrystals do attach to the surface. With tapping mode AFM, we show that these nanocrystals can easily be moved along the surface, a clear indication of weak adsorption. This is, in clear contrast to the nanocrystals attached to a sulfide-terminated surface, which are chemically bound.

Acknowledgements

We acknowledge Stephan Zevenhuizen for technical assistance.

References

[1] C. Joachim, J.K. Gimzewski, A. Aviram, Nature 408 (2000) 541.

[2] D. Porath, A. Bezryadin, S. De Vries, C. Dekker, Nature 403 (2000) 635.
[3] Z. Yao, C.L. Kane, C. Dekker, Phys. Rev. Lett. 84 (2000) 2941.
[4] S.J. Tans, C. Dekker, Nature 404 (2000) 834.
[5] J. Chen, M.A. Reed, A.M. Rawlett, J.M. Tour, Science 286 (1999) 1550.
[6] M.A. Reed, C. Zhou, C.J. Muller, T.P. Burgin, J.M. Tour, Science 278 (1997) 252.
[7] P.S. Weiss, L.A. Bumm, T.D. Dunbar, T.P. Burgin, J.M. Tour, D.L. Allara, Ann. NY Acad. Sci. 852 (1998) 145.
[8] E.P.A.M. Bakkers, A.W. Marsman, L.W. Jenneskens, D. Vanmaekelbergh, Angew. Chem. Int. Ed. 39 (2000) 2297.
[9] E.P.A.M. Bakkers, A.L. Roest, A.W. Marsman, L.W. Jenneskens, L.I. De Jong-Van Steensel, J.J. Kelly, D. Vanmaekelbergh, J. Phys. Chem. B. 104 (2000) 7266.
[10] D.I. Gittins, D. Bethell, D.J. Schiffrin, R.J. Nichols, Nature 408 (2000) 67.
[11] F.J. Hoogesteger, R.W.A. Havenith, J.W. Zwikker, L.W. Jenneskens, H. Kooijman, N. Veldman, A.L. Spek, J. Org. Chem. 60 (1995) 4375.
[12] F.J. Hoogesteger, D.M. Grove, L.W. Jenneskens, T.J.M. deBruin, B.A.J. Jansen, J. Chem. Soc., Perkin Trans. 2 (1996) 2327.
[13] A.W. Marsman, R.W.A. Havenith, S. Bethke, L.W. Jenneskens, R. Gleiter, J.H. van Lenthe, M. Lutz, A.L. Spek, J. Org. Chem. 65 (2000) 4584.
[14] A.W. Marsman, R.W.A. Havenith, S. Bethke, L.W. Jenneskens, R. Gleiter, J.H. van Lenthe, Eur. J. Org. Chem. (2000) 2629.
[15] G. Frens, Nature (Phys. Sci.) 241 (1972) 20.
[16] D. Eberhardt, E. Santos, W. Schmickler, J. Electroanal. Chem. 419 (1996) 23.
[17] T. Pajkossy, J. Electroanal. Chem. 364 (1994) 111.
[18] A. Hamelin, T. Vitanov, E. Sevastyanov, A. Popov, J. Electroanal. Chem. 145 (1983) 225.
[19] T. Pajkossy, T. Wandlowski, D.M. Kolb, J. Electroanal. Chem. 414 (1996) 209.
[20] J. Lecoeur, A. Hamelin, CR Acad. Sci. 279C (1974) 1081.
[21] J. Lecoeur, C. Sella, L. Tertain, A. Hamelin, CR Acad. Sci. 280C (1975) 247.
[22] J. Lecoeur, C. Sella, J.C. Martin, L. Tertain, J. Deschamps, CR Acad. Sci. 281C (1975) 71.
[23] A. Hamelin, J. Lecoeur, Surf. Sci. 57 (1976) 771.
[24] J. Lecoeur, J. Andro, R. Parsons, Surf. Sci. 114 (1982) 320.
[25] M.J. Esplandiu, H. Hagenstrom, D.M. Kolb, Langmuir 17 (2001) 828.
[26] C.E.D. Chidsey, D.N. Loiacono, Langmuir 6 (1990) 682.
[27] C.A. Widrig, C. Chung, M.D. Porter, J. Electroanal. Chem. 310 (1991) 335.
[28] R.P. Janek, W.R. Fawcett, A. Ulman, Langmuir 14 (1998) 3011.
[29] N.D. Lang, W. Kohn, Phys. Rev. B 1 (1970) 4555.
[30] W. Schmickler, Chem. Rev. 96 (1996) 3177.
[31] C.E.D. Chidsey, Science 251 (1991) 919.
[32] A. Ulman, Chem. Rev. 96 (1996) 1533.